Atmos. Chem. Phys. Discuss., 11, 16465–16497, 2011
www.atmos-chem-phys-discuss.net/11/16465/2011/
doi:10.5194/acpd-11-16465-2011

Atmospheric Chemistry and Physics Discussions

Using a mobile laboratory to characterize the distribution and transport of sulfur dioxide in and around Beijing

M. Wang[1,*], T. Zhu[1], J. P. Zhang[2], Q. H. Zhang[2], W. W. Lin[1,*], Y. Li[3], and Z. F. Wang[4]

[1]State Key Laboratory of Environmental Simulation and Pollution Control, College of Environmental Sciences and Engineering, Peking University, Beijing, 100871, China
[2]Department of Atmospheric and Oceanic Sciences, School of Physics, Peking University, Beijing, 100871, China
[3]Chinese Academy of Meteorological Science, Beijing, 100081, China
[4]Institute of Atmospheric Physics, Chinese Academy of Sciences, Beijing, China
[*]now at: Institute for Risk Assessment Sciences, Utrecht University, The Netherlands

Received: 30 March 2011 – Accepted: 10 May 2011 – Published: 6 June 2011

Correspondence to: T. Zhu (tzhu@pku.edu.cn)

Published by Copernicus Publications on behalf of the European Geosciences Union.

Abstract

Megacities are places with intensive human activity and energy consumption. To reduce air pollution, many megacities have relocated energy supplies and polluted industries to their outer regions. However, regional transport then becomes an important source of air pollution in megacities. To improve air quality before and during the 2008 Beijing Olympics, a wide range of control strategies were implemented, including the relocation of polluting industries. High sulfur dioxide (SO_2) concentrations were occasionally observed during this period. Potential sources from southern regions of Beijing were indicated by backward trajectories and urban/rural stationary measurements, but direct evidence was lacking. Here we used a mobile laboratory to characterize the spatial distribution and regional transport of SO_2 to Beijing during the Campaign for Air Quality Research in Beijing and the Surrounding Region (CAREBEIJING)-2008. Among the five days chosen for the case studies during the Olympic air pollution control period, four had high SO_2 concentrations (6, 20 August and 3, 4 September 2008) while one had low SO_2 concentration (11 September 2008). The average values of SO_2 during the low SO_2 concentration day were 3.9 ppb, much lower than during the high concentration days (7.8 ppb). This result implied an impact by regional transport from outside Beijing. During these days, we captured transport events of SO_2 from areas south of Beijing, with a clear decrease in SO_2 concentrations southeast of the 6th to 4th Ring Roads around Beijing and along the 140 km highway from Tianjin to Beijing. The influx of SO_2 through the 4th to 6th Ring Roads ranged from 2.07 to 4.64 $kg\,s^{-1}$ on 4 September and 0.21 to 1.56 $kg\,s^{-1}$ on 20 August 2008. Locally emitted SO_2 from a source located along Jingshi Highway outside the southwest section of the 5th Ring Road of Beijing was identified using wind field data generated by the Weather Research and Forecasting model and the measured particle size distribution, with an estimated flux of 0.11 $kg\,s^{-1}$ to Beijing.

ACPD

11, 16465–16497, 2011

1 Introduction

Sulfur dioxide (SO_2) is one of the most important precursors of secondary aerosols in the atmosphere. It is responsible for severe air pollution, leading to degraded visibility, changes in the radiation budget, and acid rain (Wang et al., 2008; Zhang et al., 2004a; Ramanathan and Crutzen, 2003). In addition, SO_2 is harmful to human health (Brunekreef and Holgate, 2002) and may cause increased respiratory diseases, reduced pulmonary function, low birth weight, and mortality (Xu et al., 1998).

Rapid economic development, industrialization, and urbanization have occurred within and around the megacity of Beijing, increasing demands for fossil fuel consumption (Ohara et al., 2007), which is the main source of SO_2. In 2008, the annual average energy consumption levels in Beijing, Tianjin, and the surrounding provinces of Heibei, Shanxi, and Shandong were 63.4 (Beijing Statistical Yearbook, 2009), 53.6 (Tianjin Statistical Yearbook, 2009), 242.2 (Hebei Statistical Yearbook, 2009), 268.8 (Shanxi Statistical Yearbook, 2009), and 125.1 (Shandong Statistical Yearbook, 2009) million tons of standard coal, respectively. To improve air quality and maintain clean air throughout the 2008 Beijing Olympics Games, Beijing municipal government implemented comprehensive long- and short-term air pollution control measures. The measures included moving heavy polluters out of the city, using low sulfur coal and high standard fuel, reducing the number of on-road vehicles, and freezing construction activities before and during the Olympics Games. While significant decreases in SO_2 were reported during the Olympics (Wang et al., 2009a, b; Qin et al., 2009), periods with relatively high SO_2 concentration occasionally occurred during the Olympic period, suggesting an important role of the regional transport of SO_2 emitted outside Beijing.

Previous studies have reported that SO_2 in Beijing is contributed by both local emission and regional transport (Zhang et al., 2004b; Xu et al., 2004; Sun et al., 2004). Rural/urban stationary (Liu et al., 2008; Guo et al., 2010) and tower observations (Sun et al., 2009) in Beijing have revealed that high wind speeds from southern areas might play a vital role in the increase of SO_2 concentrations in Beijing. An et al. (2007) used

ACPD
11, 16465–16497, 2011

the Community Multiscale Air Quality (CMAQ) model to simulate the regional transport of SO_2 and its flux pathway during a heavy pollution episode. They estimated that the southeast and southern areas of Beijing contributed 26 % and 18 % of SO_2 to the city. However, due to uncertainties in the SO_2 emission inventory outside Beijing, it is difficult to model the dispersion and transport of SO_2 accurately on small scales (Matsui et al., 2009). Thus, direct evidence from spatial distribution measurements is required.

Aircraft-based measurement with fast response instruments is a suitable approach to both studying the spatial distribution and quantifying the regional transport flux of SO_2 (Wang et al., 2006; Matvev et al., 2002; Beryrich et al., 1998). In northern China (where Beijing is located), research on SO_2 transport using aircraft measurements has focused on large-scale processes (Li et al., 2010; Ma et al., 2010; Ding et al., 2009) in the upper boundary layer or in the free troposphere. Given the high cost of aircraft measurement and difficulties in obtaining navigation approval, on-road measurement from mobile laboratories is an optimal method for ground-based spatial distribution measurement. On-road measurement platforms have been specifically designed and used for two types of applications: examination of the temporal-spatial variations in air pollutants (Bukowiecki et al., 2002; Weijers et al., 2004) and quantification of local emissions and regional transport flux (Johansson et al., 2009; Rivera et al., 2009). Johansson et al. (2008) and Li et al. (2009) calculated SO_2 fluxes from local emissions in Beijing using mobile-based mini-differential optical absorption spectroscopy (DOAS) around the 5th Ring Road of Beijing. However, these calculations were only based on column concentrations of SO_2. There is hence a lack of information on the ground level transport and concentrations of other pollutants.

Here we used an on-road mobile laboratory to measure the spatial distribution of SO_2 concentrations and identify transport processes in the southern part of Beijing. These observations were part of the Campaign for Air Quality Research in Beijing and the Surrounding Region-2008 (CAREBEIJIING)-2008. The flux of SO_2 from both local emission and regional transport was estimated using wind field data from the WRF model version 3.1.1.

ACPD
11, 16465–16497, 2011

2 Methodology

2.1 Mobile laboratory and driving routes

Details of the setup and performance of the instruments installed in the mobile laboratory were described in our previous paper (Wang et al., 2009a). Briefly, a diesel vehicle (IVECO Turin V) was selected as the mobile platform. To minimize the loss of particles in the sampling inlet, an isokinetics inlet system was designed to enhance the sampling efficiency. The instruments onboard provided data on the concentrations of gaseous pollutants (NO-NO_2-NO_x, SO_2, CO, CO_2, O_3) (ECOTECH, Australia), black carbon (MAAP, THERMO, USA), particle surface area (Nanoparticle surface area monitor, TSI, USA), particle size distribution (SMPS, DMA 3080 and CPC 3550, TSI, USA), and volatile organic compounds (VOCs; PTR-MS, IONICON, Austria). In this paper only the data of SO_2 and SMPS were used (Table 2). The time resolutions of SO_2 and SMPS data were 10 s and 2 min, respectively. Additional instruments included a Global Positioning System (GPS) and meteorological parameters (temperature, humidity, and pressure). The driving speed was $60 \pm 5\,km\,h^{-1}$.

To characterize the spatial distribution of SO_2 and to investigate the regional transport progress of SO_2 to Beijing, routes were specially designed at local scale around the south area of Beijing, and at regional scale between Beijing and Tianjin megacities (Fig. 1). The details of routes and monitoring information are listed in Table 1. In general, five days were chosen for the measurements, with four days (6, 20 August and 3, 4 September 2008) showing high SO_2 concentrations and one day showing low SO_2 concentration (11 September 2008). We first selected routes 1 and 2 along the southeast of the Ring Roads to map the SO_2 spatial distribution within the city of Beijing. The Ring Roads covers a wide scope from the urban area to the city center and thus is preferable to investigate the transport of SO_2 at local scale. Because of the limited battery power of the instruments installed on the platform, observations in the mornings and afternoons were conducted on different days. To illustrate the spatial distribution and transport of SO_2 between two megacities (Beijing and Tianjin), we

ACPD
11, 16465–16497, 2011

selected a newly built highway (Jingjintang II) between the two cities. The highway was far from industrialized areas, and because it was newly built, it had few cars driving on it during the Olympics. Thus the anthropogenic contribution from vehicular and industrial emissions was low, and the air pollutant levels were comparable to those of background air (Wang et al., 2009a). This unique feature was favorable for studying the air mass transport.

Continuous measurement was also conducted along the southwest of the 5th Ring Road and part of the 6th Ring Road in the southern area, where high-density industry is located, as shown in Fig. 1b (blue line). The characteristics of the SO_2 distribution and its local and regional emission sources surrounding the southwest of Beijing were reported previously (Wang et al., 2009a). Here we added wind field and particle size distribution data for a better understanding the distribution and emission sources of SO_2.

2.2 Ground-based meteorological and SO_2 measurements

Concentrations of SO_2 were simultaneously measured at three intensive monitoring stations before, during, and after the Olympics air pollution control period. The PKU station was in an urban station located at Peking University, Beijing (39.99° N, 116.31° E); YuFa (YF, 39.51° N, 116.31° E) and YongLeDian (YLD, 39.75° N, 116.73° E) were rural stations representing the regional background. They were located approximately 50 km to the south and southeast of Beijing. In addition, 11 meteorological stations (blue stars in Fig. 1) of the Chinese Academy of Meteorological Sciences (CAMS) were selected for meteorological data analysis. Table 2 shows measurement parameters and instruments at each station.

To ensure that data between different stations were comparable, the SO_2 analyzers (Ecotech, 9850B, Australia) in all the stations were automatically calibrated between 00:00 and 01:00 every day using the same certified calibration standard (50 ppb, accuracy 3 %, diluted with N_2, Beijing Huayuan Gas Chemical Industry Co., Ltd.). Calibration at five different concentrations (0 %, 20 %, 40 %, and 80 % of the detection

ACPD
11, 16465–16497, 2011

range) was performed each time. Meanwhile, calibrations of the SO_2 analyzer on the mobile laboratory were conducted before and after each sampling trip using similar procedures as at the stations. Intercomparison of SO_2 concentrations between the mobile laboratory and PKU station was also performed. The difference between the SO_2 concentrations was within 15 %, with a correlation coefficient of 0.82 (Wang et al., 2009a).

2.3 Wind Field

2.3.1 Lagrangian trajectory simulation

The Hybrid Single Particle Lagrangian Integrated Trajectory model (HYSPLIT, version 4.9), developed by US National Oceanic and Atmospheric Administration (NOAA) Air Resources Laboratory (ARL), was used to calculate the forward and backward trajectories from or to the stations in Beijing (Draxler and Rolph, 2003). Backward trajectories were computed once every 6 h for 24 h (1 day) at a selected height of 10 m above ground level for 45 days from 1 August to 15 September, 2008 and were grouped by cluster analysis of the model. A Global Data Assimilation System (GDAS) archive meteorological database was chosen to run the trajectory model, which had 1°×1° horizontal resolution. The horizontal resolution of the model is 1°×1°, which is enough to distinguish the original regions of the air masses in our study.

2.3.2 Weather Research and Forecasting (WRF) simulation

Direct measurements of wind speed and wind direction from the mobile lab during driving may lead to large deviations in the estimation of pollutant fluxes (Johansson, 2009). Here we used the WRF model version 3.1.1 to conduct mesoscale meteorological simulations for high-resolution wind fields and planetary boundary layer height (PBL) during the measurement periods. The WRF modeling system is a next-generation mesoscale numerical weather forecast and simulation system that includes

ACPD
11, 16465–16497, 2011

the Advanced Research dynamics solver. A detailed description of the WRF model can be found on the WRF web-site http://www.wrf-model.org/index.php, as well as in our Supplement.

Here the horizontal resolution of the model was 1 km × 1 km. Four domains were used for the WRF calculation (Fig. S1). The averaged concentrations of SO_2 were calculated based on each grid unit (1×1 km in Figs. 5 and 7, 2 × 2 km in Fig. 6). The bottom level reaching 18–20 m above the surface was selected for meteorological analysis. WRF model can simulated backward trajectories with high spatial, however, to identify the main original locations of the air masses during the measurement period and classified them into regions, it is not necessary to use WRF model for such a high resolution tracks which may take much longer time than the Hysplit model.

Comparing the WRF modeling results with the observations from meteorological stations involved in each domain during the measurement periods, we found close agreement in the wind directions, with $R = 0.83$. The wind speed had a relatively low correlation coefficient ($R = 0.66$) (Fig. S2). This could be contributed to the complicated land use in Beijing in which the local turbulences were not only influence the accuracy of the measured data in the meteorological stations (near the ground level where high buildings surround) but also challenge the predictive power of the model. However, given that most of the mobile routes were conducted in rural area, then we used just the rural sites to calculate the correlation between model and measurements (Fig. S2), and found the correlation coefficient increased significantly both for the wind speed ($R = 0.83$) and wind direction ($R = 0.89$)

The WRF model applied the newly updated land use initialized from MODIS and contains high densities of the wind fields in the vertical level (10 layers in 1000 m) and horizontal level (1 by 1 km). These improvements of the model lead us to believe that the model is able to produce a reliable spatial distribution of the wind field.

Hourly averaged WRF predicted PBL were compared with the temporal variations of aerosol extinction coefficient retrieved from Lidar measurement (Figs. S3, S4). We selected three days (6, 20 August and 11 September, 2008) with clear sky well mixed

ACPD
11, 16465–16497, 2011

convective condition; the measurement during these days could provide sufficient variation distributions of extinction coefficients. Figures S3 and S4 show that the model calculated PBL was generally in agreement with with the top boundary of the extinction coefficients during the measurement period, even though difference remained, this could be the major source of the flux uncertainty.

2.4 Assessment of the regional influx of SO_2

Quantitative assessment of SO_2 flux has been well established by the design of specified routes encircling target sources (Wang et al., 2006; Rivera et al., 2009; Johansson et al., 2008) or crossing frontiers perpendicular to the horizontal wind direction (Beryrich et al., 1998; Matvev et al., 2002). In this study, we carefully designed sector-routes on 20 August (route 1) and 4 September (route 2), so that the mobile tracks could traverse the wind direction. To calculate the transport flux outside Beijing, a simple formula based on the above measurement approach with the wind vector towards Beijing was used:

$$\text{Flux}\ (\text{kg s}^{-1}) = \sum_{i=1}^{n} C_i\ (\mu\text{g m}^{-3}) \cdot V_i (\text{m s}^{-1}) \cdot \text{Sin}\theta_i \cdot H_i(m) \cdot d_i(m) \times 10^{-9} (\text{kg}\,\mu\text{g}^{-1}) \quad (1)$$

where

Flux – the total SO_2 flux across the ring road with n $1 \times 1\ \text{km}^2$ unit cells (kg s^{-1})

C_i – the mean concentration of SO_2 $(\mu\text{g m}^{-3})$ in the i-th grid $(1 \times 1\ \text{km}^2)$

θ_i – the angle between wind direction and the driving route in the i-th grid $(1 \times 1\ \text{km}^2)$

V_i – wind speed (m s^{-1}) in the i-th grid $(1 \times 1\ \text{km}^2)$ generated by WRF output.

H – mixing layer height (m) in the i-th grid $(1 \times 1\ \text{km}^2)$ generated by WRF output

ACPD
11, 16465–16497, 2011

n – total grids ($1 \times 1\,km^2$) of each traverse path.

d_i – the transect length (m) of the mobile route in the i-th grid ($1 \times 1\,km^2$).

The principles of the flux calculations have been mentioned in Supplement S5. To estimate fluxes based on Eq. (1), two hypotheses were necessary: (1) wind speed and direction were constant during the hour (the hourly mean wind field was used), (2) the atmospheric boundary layer was stable and well-mixed during the measurement period, and the vertical distributions of SO_2 concentrations were homogenous.

3 Results and discussion

3.1 SO_2 concentration time series

Figure 2 shows the time series of SO_2 concentration and the air pollution index (API) from the three stations during the air pollution control period. The API data were from the Beijing Municipal Environmental Protection Bureau (EPB) and can be downloaded at http://www.bjepb.gov.cn/. These data gave the air pollution levels of particulate matter (PM_{10}), SO_2, and nitrogen dioxide (NO_2). API levels under 50 and 100 meant that the air quality met National Ambient Air Quality Standard Levels I and II. An API over 100 implies potentially adverse effects on the population.

In general, SO_2 concentrations were low during the Olympic air pollution control period (8 to 24 August 2008) at all stations, with average values of 5.8 ppb in the city and 3.2 ppb in rural areas. The mean API varied around 50. However, there were three periods with high SO_2 concentration at all stations: 3~10 August, 19~30 August, and 2~8 September (Fig. 2). During these periods SO_2 concentration varied dramatically, with diurnal peak levels higher than 15 ppb. These trends were in agreement with API variations, for which mean values in the three periods were 80, 75, and 66, respectively. The maximum API level was around 100. During the 2008 Beijing Olympics period, most of the SO_2 emission sources were strictly controlled within and around

ACPD
11, 16465–16497, 2011

Beijing (Wang et al., 2009a); therefore, we assumed that local emission within Beijing city was not a major source of the increase in SO_2. Hence regional transport of SO_2 under appropriate meteorological conditions, e.g., wind speed and wind direction, should have been the major cause.

To further investigate the possible source of the observed SO_2, back trajectories were used to examine the air masses arriving in Beijing during the measurement period. A total of 184 trajectories (4 per day) were generated from the center of Beijing and then classified into four groups by cluster analysis. This revealed four typical source regions. Figure 3 shows the three clusters that derived from regional transport outside Beijing. The first group of trajectories (blue) originated from the Bohai Sea in the southeast of China and then moved over the Tianjin and Tangshan areas. The second group (green) was southerly from inland China, passing over Henan and Hebei provinces. The third group (red) was from the northwest of Inner Mongolia and the northeast regions of China. The last group (not shown here) travelled locally around Beijing city. Among the 184 trajectories, clusters 1, 2, 3, and 4 accounted for 22 %, 28 %, 26 %, and 24 % of all the trajectories, respectively. The 24 hour trajectories of clusters 1 and 2 were short, due to the slow wind, and thus SO_2 might have accumulated in Beijing. In contrast, the long trajectories of cluster 3 indicated strong winds from the northern area, which brought clean air and were favorable to air dispersion. Figure 4 shows the mean SO_2 concentration and API value in Beijing for each trajectory cluster. As expected, high SO_2 concentrations and API values were observed on the same days as the trajectory clusters 1 and 2. The average SO_2 concentrations ranged from 5.7 to 7.8 ppb, while the API values varied from 64.9 to 75.2. Trajectory clusters 3 and 4 were associated with low SO_2 concentrations and API values, which ranged from 3.9 to 4.8 ppb and 39 to 45, respectively.

Apparently, regional transport played an important role in increasing SO_2 concentrations in Beijing. To further investigate the SO_2 transport into Beijing, we used three mobile laboratory measurements to provide spatial distributions of SO_2 and to quantify its regional influx to Beijing.

ACPD
11, 16465–16497, 2011

3.2 Case studies of SO_2 spatial distribution

3.2.1 Southeastern area: routes 1 and 2

Figure 5a and b overlap the SO_2 concentration measured by the mobile laboratory and the wind field generated with the WRF model on 20 August and 4 September. The prevailing winds were from the SE and SSE with speeds of $1.2 \pm 0.2\,m\,s^{-1}$ and $3.6 \pm 1.2\,m\,s^{-1}$, respectively. The average mixing boundary layer height was 1027 ± 232 m on 20 August and 1223 ± 48 m on 4 September (Fig. S4). On both days, SO_2 concentrations had apparent horizontal gradients, increasing from urban to rural areas (Fig. 7) and clearly reflecting the transport patterns of SO_2 from the source regions in south area. It is noted that the temporal variations of SO_2 emissions may be convoluted with the spatial variability due to the driving speed of the mobile. However, since the wind speeds in both the measuring days were not fast, assuming that the SO_2 emissions during measurement period were stable and the air masses were large enough, this influence on the SO_2 distributions was low.

Figure 5 shows that high SO_2 concentrations were observed for approximately 30 km along the 5th and 6th Ring Roads, implying large-scale air mass transport. The mean value of SO_2 on 4 September was 14.9 ± 3.2 ppb, twice as high as the 6.8 ± 2.1 ppb observed on 20 August. The 48 h backward trajectory on 20 August started in the Bohai Sea and encircled the suburban and urban areas of Tianjin before reaching Beijing (Fig. S6). On 4 September (Fig. S6), however, the 48 h backward trajectory originated from the mid-eastern mainland of China, traveling northward across Hebei, Henan, and even Shandong provinces. These areas contain numerous thriving industrialized cities where anthropogenic pollutants, especially SO_2, are generated (Streets et al., 2007). Liu et al. (2010) reported the neighboring provinces around Beijing such as Shandong, Hebei and Shanxi province contribute a large amount of SO_2 emissions of China (details please see Sect. 3.4). Air masses flowing across these regions usually pick up heavy pollutants downwind, leading to high concentrations of SO_2.

ACPD
11, 16465–16497, 2011

Figure 5c and d show the distributions of SO_2 influx through the Ring Roads based on (1) and the high-resolution wind field. The flux of SO_2 on 4 September was four times higher than that on 20 August. The SO_2 in Beijing on 4 September was obviously imported from the southern region, while the pathway on 20 August was possibly from the southeast.

3.2.2 Southeastern area: routes 3 and 4 between Beijing and Tianjin

Figure 6a shows consistent decreasing trends of SO_2 concentration from Tianjin to Beijing on 3 September, under southeasterly prevailing winds, indicating the regional transport of SO_2 from relatively distant sources. The average SO_2 concentrations along route 3 were modestly high, about 23 ppb. The maximum SO_2 concentration over 40 ppb was observed in the industrial centers of Tianjin, Tanggu, and Hangu (Fig. 7). In contrast, SO_2 concentrations had a very different distribution on 11 September (Fig. 6b), when the northwesterly wind dominated. The SO_2 concentrations were low, with an average concentration of around 5 ppb along route 4 (Fig. 7), while SO_2 concentrations in Beijing and Tianjin were relatively high. This suggests that SO_2 in the cities came mainly from local SO_2 emission sources.

While the wind field on 3 September was similar to that on 20 August and 4 September, the mean SO_2 concentrations on the southeast of the 5th ring road differed between the three days, e.g. 7.5 ppb, 13.2 ppb, and 16.2 ppb on 20 August, 3 September and 4 September, respectively. This difference of the SO_2 concentrations can be explained by the reason that 20 August was still in the Olympic period, when air pollution was strictly controlled. SO_2 emissions on August 20 were expected less than that on 3 and 4 September. This difference can also be found from the stationary measurements as well as API variations in Fig. 1, in which the SO_2 concentrations and API values on 20 August were lower than that on 3 and 4 September.

Figure 6c and d show the distributions of the SO_2 flux along route 3 from Beijing to Tianjin on 3 September and route 4 from Tianjin to Beijing on 11 September. Since wind directions in both days were mostly towards Beijing or Tianjin, we simplify the flux

ACPD
11, 16465–16497, 2011

formula by using the product of mean SO_2 concentration in each cell and the measured wind speed to represent the SO_2 flux though the individual grid unit ($2 \times 2\,km^2$). The wind speeds on both days were similar: $2.38 \pm 0.27\,m\,s^{-1}$ and $2.04 \pm 0.15\,m\,s^{-1}$, respectively. The boundary layer was high on 3 September ($1220 \pm 150\,m$) and relatively low on 11 September ($833 \pm 267\,m$). The flux of SO_2 imported to Beijing on 3 September was $124.3\,g\,s^{-1}$ in $2 \times 2\,km^2$ grid units, much higher than the flux to Tianjin on 11 September ($24.2\,g\,s^{-1}$ in $2 \times 2\,km^2$ grid units).

3.2.3 Southwestern area: route 5 surrounding Beijing

We previously reported high concentrations of SO_2 and other pollutants in the Shijingshan district and along Jingshi Highway on 6 August 2008 and suggested this pollution was possibly from both local emission and regional transport (Wang et al., 2009a), but we had no further evidence to support this suggestion. In the particle number size distributions (Fig. 8c), we found bimodality with a remarkably high peak of ultrafine particle number concentrations in the 14.9–100 nm range and a smaller peak in the range larger than 100 nm, along Jingshi Highway. A similar observation was found in the Shijingshan district, but with lower particle number concentration peaks. Local emissions sources such as traffic exhaust, industrial emission, and biomass burning were identified as the major contributors to the particle number concentrations in the small range, while the larger size particles were "aged", having formed during regional transport. Thus, we believe that the increase in SO_2 recorded along Jingshi Highway (Fig. 8b) was caused by both local emissions and regional transport.

To further investigate the high SO_2 concentrations in the Shijingshan district, we used the high-resolution wind field from the WRF simulation. As shown in Fig. 8a, on 6 August the observation along Jingshi Highway was dominated by winds flowing toward the northeast area, with the Shijingshan district located precisely downwind. Pollutants dispersed along the downwind direction from Jingshi Highway, leading to a high peak in SO_2 concentration across the Shijingshan district (see Fig. 8b dashed boxes).

ACPD
11, 16465–16497, 2011

The first peak of SO_2 at Shijingshan section shows clearly an overlay of the local emission and regional transported SO_2. We used a simple spline interpolation to separate the SO_2 from local emission (shaded area of the first Shijianshan peak in Fig. 8b) and regional transport (underneath the red dots of the first Shijianshan peak in Fig. 8b). The SO_2 from local emission was estimated by extracting the regional background of SO_2 from the measured SO_2 concentration. With this, we estimated the local emission from Jingshi Highway to the Shijingshan district represented 16 % of the measured SO_2 concentrations.

3.3 Estimate of SO_2 influx to Beijing

Table 3 lists the flux of SO_2 through the Ring Roads on 6 and 20 August and 4 September calculated with (1). The SO_2 flux on the 5th Ring Road on 6 August was determined as 1.64 kg s^{-1}, with 2.9 m s^{-1} wind speed and 1140 ± 233 m boundary layer height. The flux of local emission on Jingshi Highway was assessed by calculating the downwind SO_2 traverse at the southwestern 5th Ring Road in the Shijingshan district, generating a SO_2 flux of 0.11 kg s^{-1}. The flux of SO_2 increased from the 4th to 6th Ring Roads, from 0.21 to 1.56 kg s^{-1} on 20 August and 2.07 to 4.64 kg s^{-1} on 4 September. The large difference between the estimated fluxes of SO_2 could be explained by the higher SO_2 concentrations and stronger winds on 4 September compared with those on 20 August.

Uncertainty in estimates of the SO_2 flux in this study may came from the uncertainties in both horizontal and vertical distributions of wind profiles, the height of boundary layers, and the time interval across the plume (Wang et al., 2008). The horizontal differences in wind speed and direction found by the WRF model were 19 % and 7.5 % with regard to the station monitoring data. Zhu et al. (2010) observed a homogeneous vertical distribution of SO_2 in daytime in Beijing with DOAS measurements, which suggested our assumption of homogeneous vertical distribution of SO_2 is justified. However, uncertainties in vertical wind profile and PBL were difficult to estimate because

ACPD
11, 16465–16497, 2011

of the lack of measurement data. Given the large spatial variation of SO_2 emission in neighboring regions of Beijing (Sect. 3.4), we are confident that our flux calculations are reasonable with acceptable uncertainty.

3.4 Comparison of measured SO_2 fluxes with emission inventory

Table 4 shows a comparison of our results with published emission inventory from the provinces surrounding Beijing. Given a rapid increase of the emissions in China, we choose the most recent report of the emission inventory in 2007 (Liu et al., 2010), which was based on the INTEX-B inventory. The sum of the emissions from the power plant, industry, domestic and traffic sources in provinces surrounding Beijing were listed in Table 4.

As shown in Table 4, Beijing and Tianjin have the lowest emission of SO_2, while Shandong province has the highest SO_2 emission, followed by Hebei and Shanxi provinces. The SO_2 emission from Shandon was tenfold higher than that in Beijing and could contributed to the SO_2 concentration in Beijing under south or southeast winds. The Hebei province is in proximity to Beijing with high SO_2 emission, and may contribute more to Beijing SO_2 concentrations, due to shorter distance compared to Shandon province. The emissions from Tianjin city was much lower than the emissions from the other provinces, which may partially account for the relatively low SO_2 concentrations on 20 August when southeastern wind dominated.

We extrapolate the SO_2 flux measured on 20 August and 4 September at the ring roads, to the annual SO_2 flux into Beijing. Table 4 shows that the annual influxes of SO_2 through the southeast of the 6th ring road to Beijing could be as high as 146.3 Gg yr^{-1} and 65.3 Gg yr^{-1} on the 4th ring road. This is about one third or equivalent to the SO_2 emission in Beijing, suggesting the transport of SO_2 is of pivotal importance to the SO_2 concentration in Beijing. Apparently, high uncertainties are associated with the SO_2 flux measurements and this extrapolation, but our results gives a relative importance of the SO_2 transport similar as previously reported model estimation of a heavy pollution episode (An et al., 2007).

ACPD
11, 16465–16497, 2011

4 Conclusions

We used a mobile laboratory to identify and assess the transport processes and emission sources of SO_2 surrounding Beijing in combination with the wind field distribution. The measurements were conducted as a part of the CAREBeijing-2008 campaign from August to September 2008 and covered the southeast and southwest areas outside Beijing.

Continuous measurements at the PKU urban station and the YuFa and YongLeDian rural stations were performed before, during, and after the comprehensive control period. Three potential polluted periods were identified, with short backwards trajectories from the south and southeast areas outside Beijing.

Mobile monitoring was conducted to investigate the regional transport of SO_2 from the southern mainland of China. We designed three routes. The route along the southeast of the Ring Roads reflected the wide scope of the polluted plumes, while the "straight line" between Beijing and Tianjin further supported the regional transport of SO_2 over long distances. We also noticed that the plumes from the center of mainland China usually picked up pollutants along the way, leading to high concentrations on 4 September compared to those on 20 August. On 6 August, regional transport from southeast areas as well as local emissions on Jingshi Highway and their dispersion over the downwind district of Shijingshan were identified and demonstrated by WRF simulations and particle size-distribution measurements.

Using a simple method assuming constant wind speed and directions within 1 h and homogeneous vertical profiles of the well-mixed boundary layer, we found that the flux of SO_2 transported to Beijing was high on 4 September and low on 20 August. From the 4th to the 6th Ring Roads, the SO_2 flux ranged from 2.07 to 4.64,kg s^{-1} on 4 September and 0.21 to 1.56 kg s^{-1} on 20 August. Influx from the southwest on 6 August across the 5th Ring Road was 1.64 kg s^{-1}. Local emission on Jingshi Highway was roughly 0.11 kg s^{-1}. In summary, mobile monitoring is a useful approach to evaluate temporal

ACPD
11, 16465–16497, 2011

and spatial variations in SO_2 transport processes. The uncertainty of the SO_2 flux estimation can be reduced by using concurrent measured boundary layer height.

Supplementary material related to this article is available online at: http://www.atmos-chem-phys-discuss.net/11/16465/2011/acpd-11-16465-2011-supplement.pdf.

Acknowledgements. This study was supported by Beijing Environmental Protection Bureau (OITC-G08026056). We would like to thank TSI Inc. for their assistance on SMPS instrument support. Special thanks also to Chinese Meteorological Administration for meteorological data support. We also acknowledge Weili Lin and Rob Beelen for providing precious advices on back trajectory model and data analysis. Finally, we thank NOAA for the data support of the back trajectory model.

References

An, X., Zhu, T., Wang, Z., Li, C., and Wang, Y.: A modeling analysis of a heavy air pollution episode occurred in Beijing, Atmos. Chem. Phys., 7, 3103–3114, doi:10.5194/acp-7-3103-2007, 2007.

Beijing Statistical Yearbook: China Statistics Press, Beijing, China. 2009.

Beryrich, F., Grafe, H., Kuchler, W., Lindemann, C., and Schaller, E.: An obervational study of sulphur dioxide transport across the erzgebirge mountains, Atmos. Environ., 32, 1027–1038, 1998.

Brunekreef, B. and Holgate, S. T.: Air pollution and health, Lancet, 360, 1233–1242, 2002.

Bukowiecki, N., Dommen, J., Prevot, A. S. H., Richter, R., Weingartner, E., and Baltensperger, U.: A mobile pollutant measurement laboratory-measuring gas phase and aerosol ambient concentrations with high spatial and temporal resolution, Atmos. Environ., 36, 5569–5579, 2002.

Ding, A. J., Wang, T., Xue, L. K., Gao, J., Stohl, A., Lei, H. C., Jin, D. Z., Ren, Y., Wang, X. Z., Wei, X. L., Qi, Y. B., Liu, J., and Zhang, X. Q.: Transport of north china air pollution by

ACPD
11, 16465–16497, 2011

midlatitude cyclones: Case study of aircraft measurements in summer 2007, J. Geophys. Res.-Atmos., 114, D11399, doi:10.1029/2009jd012339, 2009.
Draxler, R. R. and Rolph, G. D.: Hysplit (hybrid single-particle lagrangian integrated trajectory) model access via noaa arl ready website (http://www.Arl.Noaa.Gov/ready/hysplit4.Html), NOAA Air Resources Laboratory, 2003.
Guo, S., Hu, M., Wang, Z. B., Slanina, J., and Zhao, Y. L.: Size-resolved aerosol water-soluble ionic compositions in the summer of Beijing: implication of regional secondary formation, Atmos. Chem. Phys., 10, 947–959, doi:10.5194/acp-10-947-2010, 2010.
Hebei Statistical Yearbook: China Statistics Press, Beijing, China, 2009.
Johansson, M., Galle, B., Yu, T., Tang, L., Chen, D., Li, H. J., Li, J. X., and Zhang, Y.: Quantification of total emission of air pollutants from beijing using mobile mini-doas, Atmos. Environ., 42, 6926–6933, 2008.
Johansson, M., Rivera, C., de Foy, B., Lei, W., Song, J., Zhang, Y., Galle, B., and Molina, L.: Mobile mini-DOAS measurement of the outflow of NO_2 and HCHO from Mexico City, Atmos. Chem. Phys., 9, 5647–5653, doi:10.5194/acp-9-5647-2009, 2009.
Li, A., Xie, P. H., Liu, W. Q., Liu, J. G., and Dou, K.: Studies on the determination of the flux of gaseous pollutant from an area by passive differential optical absorption spectroscopy, Spectrosc. Spect. Anal., 29, 28–32, 2009 (in Chinese).
Li, C., Krotkov, N. A., Dickerson, R. R., Li, Z. Q., Yang, K., and Chin, M.: Transport and evolution of a pollution plume from northern china: A satellite-based case study, J. Geophys. Res.-Atmos., 115, D00K03, doi:10.1029/2009jd012245, 2010.
Liu, J., Zhang, X. L., Xu, X. F., and Xu, H. H.: Comparison analysis of variation characteristics of SO_2 , NO_x, O_3 and pm2.5 between rural and urban areas, Beijing, Environm. Sci., 29, 1059–1065, 2008.
Lu, Z., Streets, D. G., Zhang, Q., Wang, S., Carmichael, G. R., Cheng, Y. F., Wei, C., Chin, M., Diehl, T., and Tan, Q.: Sulfur dioxide emissions in China and sulfur trends in East Asia since 2000, Atmos. Chem. Phys., 10, 6311–6331, doi:10.5194/acp-10-6311-2010, 2010.
Matsui, H., Koike, M., Kondo, Y., Takegawa, N., Kita, K., Miyazaki, Y., Hu, M., Chang, S. Y., Blake, D. R., Fast, J. D., Zaveri, R. A., Streets, D. G., Zhang, Q., and Zhu, T.: Spatial and temporal variations of aerosols around beijing in summer 2006: Model evaluation and source apportionment, J. Geophys. Res.-Atmos., 114, D00G13, doi:10.1029/2008JD010906, 2009.
Ma, J. Z., Chen, Y., Wang, W., Yan, P., Liu, H. J., Yang, S. Y., Hu, Z. J., and Lelieveld, J.: Strong air pollution causes widespread haze-clouds over China, J. Geophys. Res.-Atmos.,

ACPD
11, 16465–16497, 2011

115, D18204, 10.1029/2009JD013065, 2010.
Matvev, V., Dayan, U., Tass, I., and Peleg, M.: Atmospheric sulfur flux rates to and from israel, Sci. Total Environ., 291, 143–154, 2002.
Ohara, T., Akimoto, H., Kurokawa, J., Horii, N., Yamaji, K., Yan, X., and Hayasaka, T.: An Asian emission inventory of anthropogenic emission sources for the period 1980-2020, Atmos. Chem. Phys., 7, 4419–4444, doi:10.5194/acp-7-4419-2007, 2007.
Qin, M., Xie, P. H., Wu, D. X., Xu, J., Si, F. Q., Wang, M. H., Dou, K., Zhang, Y., Xiao, X., Liu, W. S., Liu, S. S., Wang, F. P., Fang, W., Liu, J. G., and Liu, W. Q.: Investigation of variation characteristics and levels of so2no2o3 and pm10 in beijing during 2008 Olympic games, Journal of Atmospheric and Environmental Optics, 4, 329–340, 2009.
Ramanathan, V., and Crutzen, P. J.: New directions: Atmospheric brown "Clouds", Atmos. Environ., 37, 4033–4035, 2003.
Rivera, C., Sosa, G., Wöhrnschimmel, H., de Foy, B., Johansson, M., and Galle, B.: Tula industrial complex (Mexico) emissions of SO_2 and NO_2 during the MCMA 2006 field campaign using a mobile mini-DOAS system, Atmos. Chem. Phys., 9, 6351–6361, doi:10.5194/acp-9-6351-2009, 2009.
Streets, D. G., Fu, J. S., Jang, C. J., Hao, J. M., He, K. B., Tang, X. Y., Zhang, Y. H., Wang, Z. F., Li, Z. P., Zhang, Q., Wang, L. T., Wang, B. Y., and Yu, C.: Air quality during the 2008 beijing olympic games, Atmos. Environ., 41, 480–492, 2007.
Shandong Statistical Yearbook: China Statistics Press, Beijing, China 2009.
Shanxi Statistical Yearbook: China Statistics Press. Beijing, China, 2009.
Sun, Y., Wang, Y. S., and Zhang, C. C.: Measurement of the vertical profile of atmospheric SO_2 during the heating period in beijing on days of high air pollution, Atmos. Environ., 43, 468–472, 2009.
Sun, Y. L., Zhuang, G. S., Wang, Y., and Han, L. H.: The airborne particulate pollution in beijing-concentration, composition, distribution and sources, Atmos. Environ., 38, 5991–6004, 2004.
Tianjin Statistical Yearbook: China Statistics Press, Beijing, China, 2009.
Wang, M., Zhu, T., Zheng, J., Zhang, R. Y., Zhang, S. Q., Xie, X. X., Han, Y. Q., and Li, Y.: Use of a mobile laboratory to evaluate changes in on-road air pollutants during the Beijing 2008 Summer Olympics, Atmos. Chem. Phys., 9, 8247–8263, doi:10.5194/acp-9-8247-2009, 2009.
Wang, P., Richter, A., Bruns, M., Burrows, J. P., Scheele, R., Junkermann, W., Heue, K.-P.,

ACPD
11, 16465–16497, 2011

Wagner, T., Platt, U., and Pundt, I.: Airborne multi-axis DOAS measurements of tropospheric SO_2 plumes in the Po-valley, Italy, Atmos. Chem. Phys., 6, 329–338, doi:10.5194/acp-6-329-2006, 2006.

Wang, W., Ren, L. H., Zhang, Y. H., Chen, J. H., Liu, H. J., Bao, L. F., Fan, S. J., and Tang, D. G.: Aircraft measurements of gaseous pollutants and particulate matter over pearl river delta in china, Atmos. Environ., 42, 6187–6202, 2008.

Wang, Y., Hao, J., McElroy, M. B., Munger, J. W., Ma, H., Chen, D., and Nielsen, C. P.: Ozone air quality during the 2008 Beijing Olympics: effectiveness of emission restrictions, Atmos. Chem. Phys., 9, 5237–5251, doi:10.5194/acp-9-5237-2009, 2009.

Weijers, E. P., Khlystov, A. Y., Kos, G. P. A., and Erisman, J. W.: Variability of particulate matter concentrations along roads and motorways determined by a moving measurement unit, Atmos. Environ., 38, 2993–3002, 2004.

Xu, X. D., Zhou, L., and Zhou, X. J.: Urban environment region influenced by surrounding sources during serious atmospheric pollution process, Sci. China Ser. D, 34, 958–966, 2004.

Xu, X. P., Wang, L. H., and Niu, T. H.: Air pollution and its health effects in beijing, Ecosyst. Health, 4, 199–209, 1998.

Zhang, M. G., Uno, I., Yoshida, Y., Xu, Y. F., Wang, Z. F., Akimoto, H., Bates, T., Quinn, T., Bandy, A., and Blomquist, B.: Transport and transformation of sulfur compounds over east asia during the trace-p and ace-asia campaigns, Atmos. Environ., 38, 6947–6959, 2004a.

Zhang, Z. G., Gao, Q. X., and Han, X. Q.: The study of pollutant transport between the cities in north china, Res. Environ. Sci., 17, 14–20, 2004b.

Zhu, Y. W., Liu, W. Q., Xie, P. H., Dou, K., Qin, M., and Si, F. Q.: Monitoring and analysis for vertical profiles of air pollutants in boundary layer of Beijing, Chinese J. Geophys.-Ch., 53, 1278–1283, 2010 (in Chinese).

ACPD
11, 16465–16497, 2011

Table 1. Mobile measurement dates and route types.

Cruise Route	Starting date time (LT)	Ending date time (LT)	Route type
Route 1	20 Aug 2008 (07:58)	20 Aug 2008 (12:50)	Southeast 2th to 6th Ring RD
Route 2	4 Sep 2008 (14:13)	4 Sep 2008 (18:22)	Southeast 4th to 6th Ring RD
Route 3	3 Sep 2008 (10:05)	3 Sep 2008 (15:13)	Beijing to Tianjin
Route 4	11 Sep 2008 (10:09)	11 Sep 2008 (14:37)	Beijing to Tianjin
Route 5	6 Aug 2008 (12:00)	6 Aug 2008 (14:50)	Southwest area outside Beijing

ACPD
11, 16465–16497, 2011

Table 2. Instrumentation performed in this study.

Station name	Instruments	Measurement species
Mobile Laboratory	SO_2 analyzer (Ecotech 9850A, Austrilia) (10 s)	SO_2
	scanning mobility particle sizer (SMPS) (3080, TSI Inc.) (2 min)	Size distribution (size 14.1–667 nm)
PKU station	SO_2 analyzer (Ecotech 9850B, Austrilia) (1 h)	SO_2
	Mete One (1∼3 h)	Wind speed, wind direction
YuFa station	SO_2 analyzer (Ecotech 9850B, Austrilia) (1h)	SO_2
	Mete One (1∼3 h)	Wind speed, wind direction
YongLeDian station	SO_2 analyzer (Ecotech 9850B, Austrilia) (1 h)	SO_2
	Mete One (1∼3 h)	Wind speed, wind direction
CAMS stations	Mete One (1∼3 h)	Wind speed, wind direction

ACPD
11, 16465–16497, 2011

Table 3. SO_2 import fluxes and local emission derived from mobile laboratory in different routes surrounding Beijing.

	SO_2 flux ($kg\,s^{-1}$)				
	4th Ring RD SE	5th Ring RD SE	6th Ring RD SE	5th Ring RD SW	Shijingshan
6 Aug 2008				1.64	0.11
20 Aug 2008	0.21	0.41	1.56		
4 Sep 2008	2.07	4.02	4.64		

ACPD
11, 16465–16497, 2011

Table 4. Comparison of the 2007 emission flux of SO_2 in provinces surrounding Beijing with the estimated SO_2 annual flux into Beijing.

Province	Ring roads	SO_2 emission ($Gg\,yr^{-1}$)	SO_2 flux ($Gg\,yr^{-1}$) 20 Aug/4 Sep	Reference
Beijing		194		Liu et al. (2010)
Tianjin		323		Liu et al. (2010)
Hebei		2481		Liu et al. (2010)
Shandong		4373		Liu et al. (2010)
Shanxi		1738		Liu et al. (2010)
	Beijing 4th Ring RD		6.6/65.3	This study
	Beijing 5th Ring RD		12.9/126.7	This study
	Beijing 6th Ring RD		49.2/146.3	This study

ACPD
11, 16465–16497, 2011

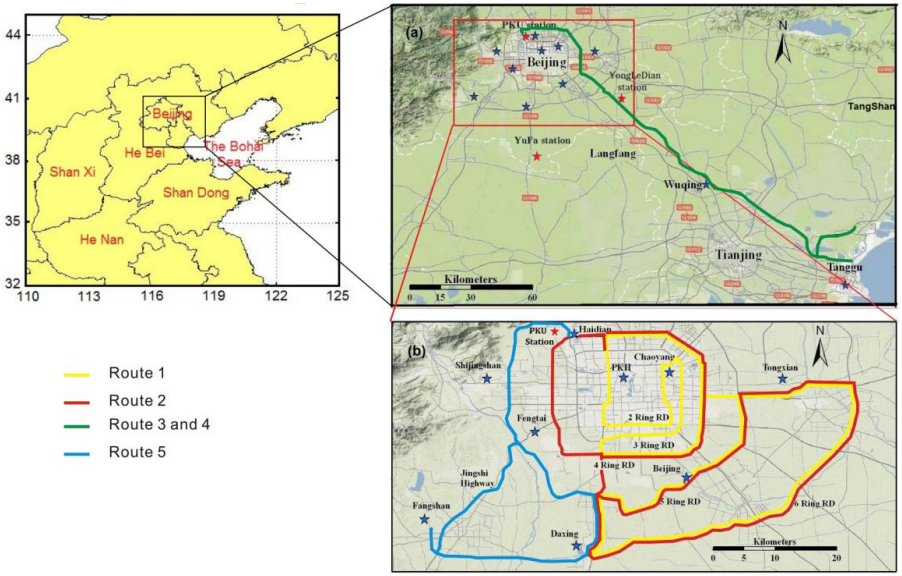

Fig. 1. Maps of the mobile monitoring areas in CAREBeijing-2008. The green track in **(a)** shows route 3 and 4 in Table 1. The red, yellow and blue tracks in **(b)** show the route 1, 2 and route 5, respectively. The red stars on the maps represent the stationary sites on SO_2 measurements and the blue stars show the CAMS meteorological stations.

ACPD
11, 16465–16497, 2011

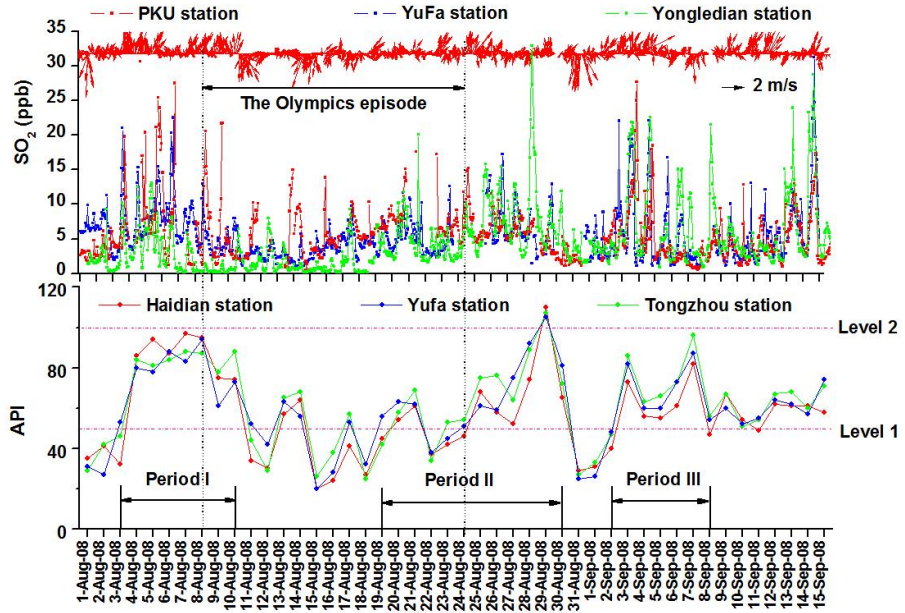

Fig. 2. Temporal variations of SO_2 concentrations at PKU, YuFa and YongLeDian stations and API values reported by Beijing EPB from 1 August to 15 September 2008. The red arrows show the wind vectors at PKU station. The dashed line of level 1 and 2 indicates the maximum of national air quality criteria I (50) and II (100), respectively. Period I, II and III show the potential SO_2 pollution periods with increase trends between 3–10 August, 19–30 August and 2–8 September.

ACPD
11, 16465–16497, 2011

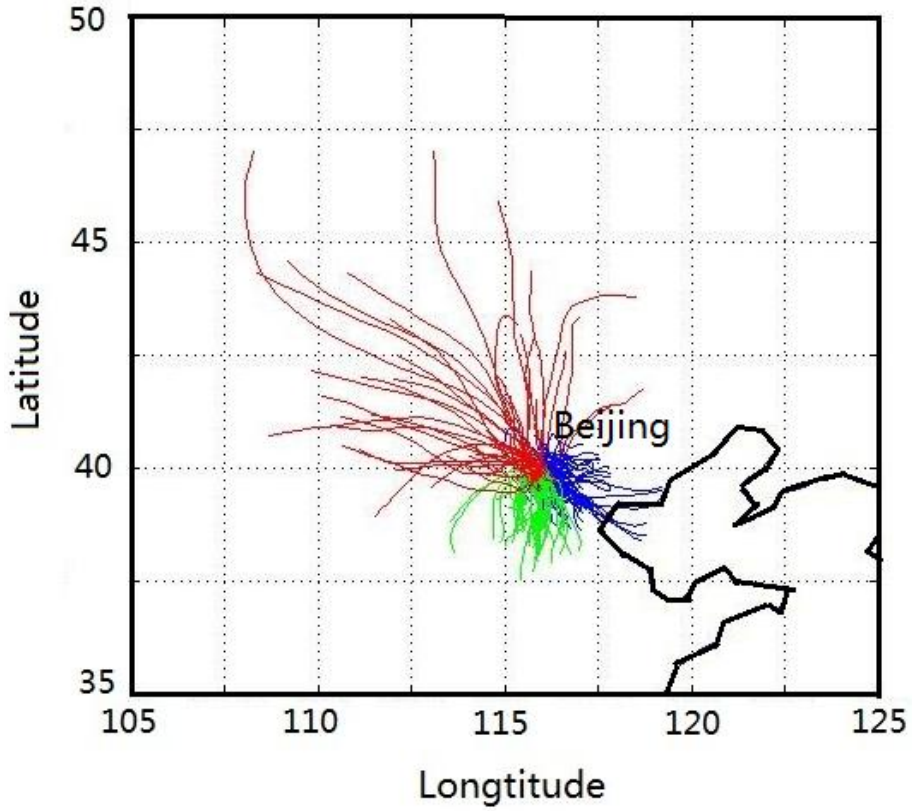

Fig. 3. Air mass backward trajectories at 10 m above ground level at Beijing from 1 August to 15 September 2008. The red, green and blue trajectories show the plumes from north, south and southeast regions.

ACPD
11, 16465–16497, 2011

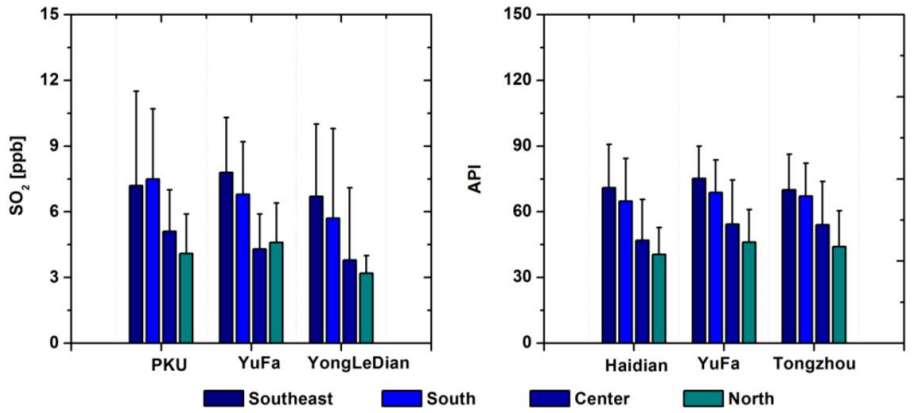

Fig. 4. The average concentrations of SO_2 and API measured at PKU (Haidian for API), YuFa (YuFa) and YongLeDian (Tongzhou) sites subdivided on the basis of four directions of backtrajectories from 1 August to 15 September 2008. The bars show the standard deivations of SO_2 concentrations and API.

ACPD
11, 16465–16497, 2011

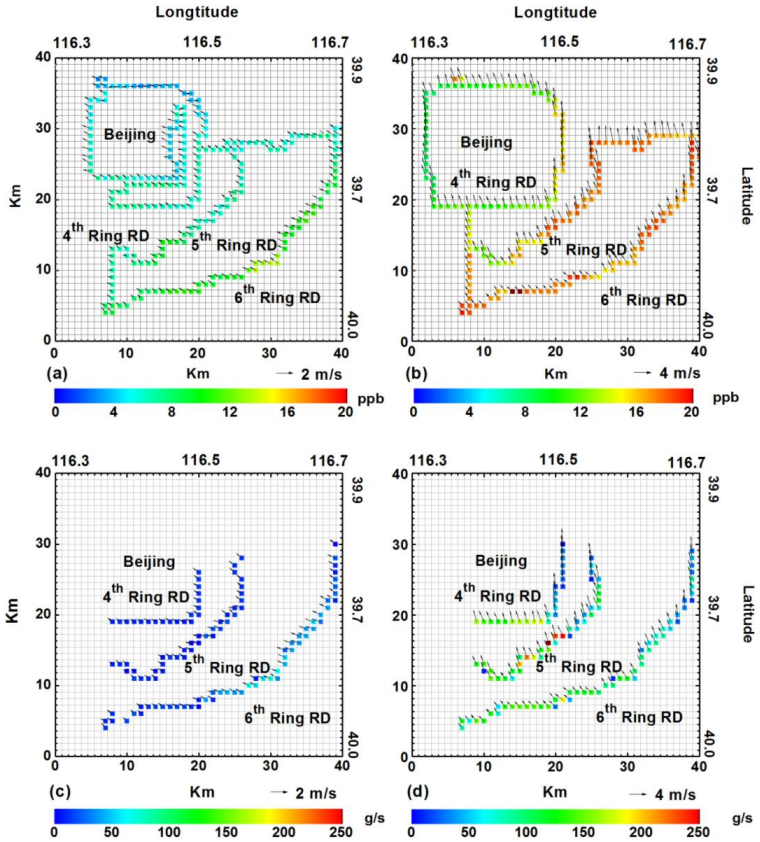

Fig. 5. The spatial distributions of SO_2 concentrations and wind field by WRF with 1 ×1 km grids resolution in southeastern areas of Beijing on **(a)** 20 August and **(b)** 4 September 2008, as well as the corresponding flux on 20 August **(c)** and 4 September 2008 **(d)**.

ACPD
11, 16465–16497, 2011

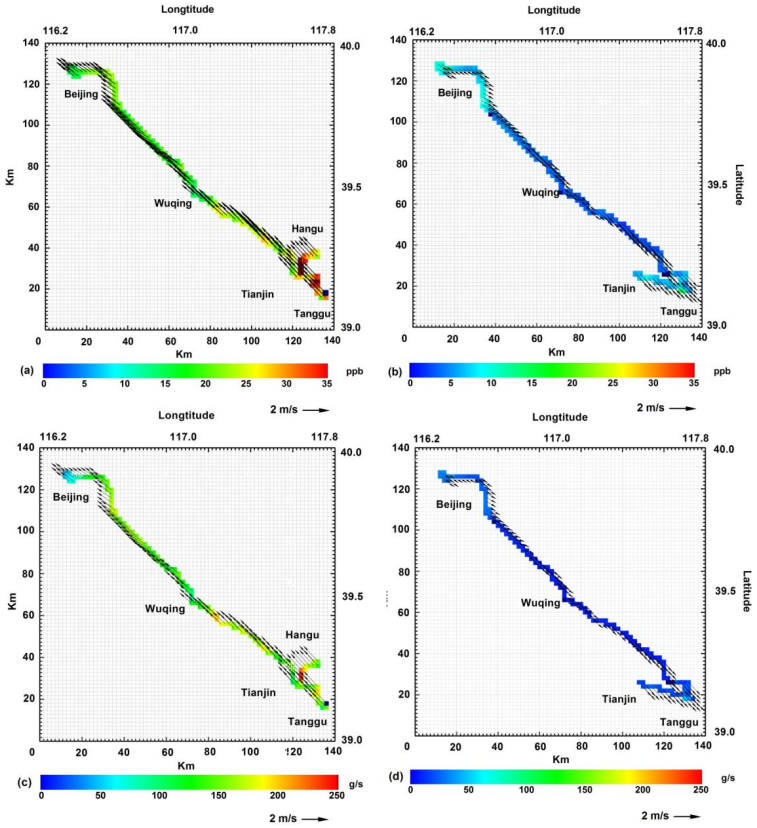

Fig. 6. The spatial distributions of SO_2 concentrations from Beijing to Tianjin on **(a)** 3 September and **(b)** 11 September 2008; the corresponding flux on 3 September and 11 September 2008 are shown in **(c)** and **(d)**.

ACPD
11, 16465–16497, 2011

Distribution and transport of sulfur dioxide

M. Wang et al.

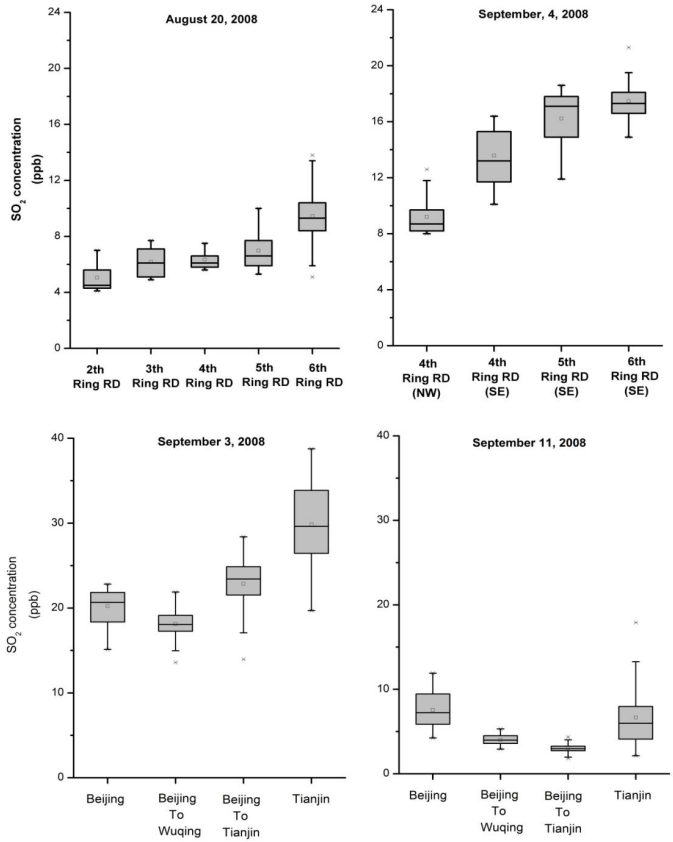

Fig. 7. Boxplots of the SO_2 concentrations on the ring roads in southeast of Beijing during the measurement periods. The small block indicates the mean value and the upper, middle and bottom layers of the box show the 75, 50, 25-th percentiles of the dataset. The bars are determined by the 5 and 95th percentiles of the dataset and "×" show the maximum and minimum values, respectively.

ACPD
11, 16465–16497, 2011

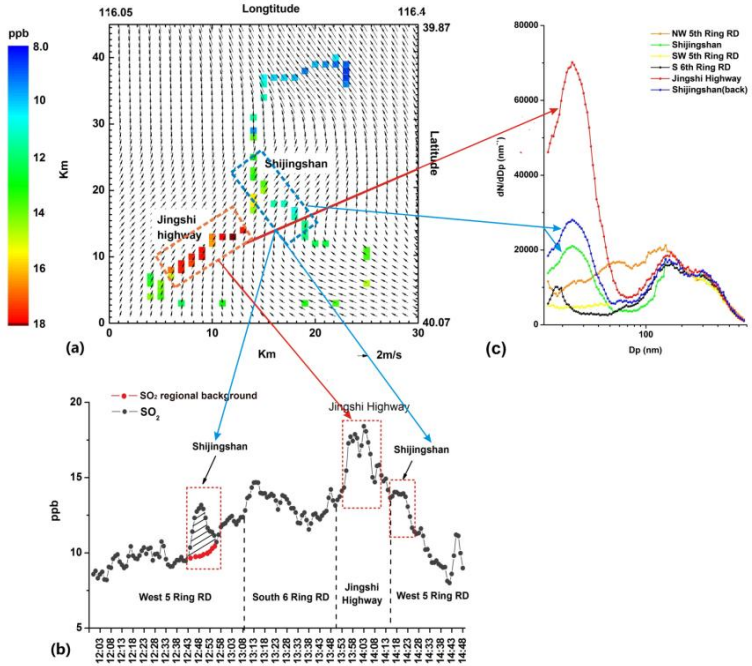

Fig. 8. **(a)** SO_2 spatial distributions and wind field by WRF with $1\times1\,km^2$ grids resolution in southwestern areas of Beijing on 6 August 2008. The dashed areas on the left and middle of the figure represent Jingshi Highway and Shijingshan district where high peak values were observed; **(b)** time series of SO_2 variations on 6 August, where the red plots and the black shades show the regional background and local emission of SO_2 across the 5th Ring Road. **(c)** SMPS particle size distributions measured in seperated areas of the route on 6 August. The red and blue arrows display the Jingshi Highway and Shijingshan districts in **(a)** corresponding to the SO_2 peak values in **(b)** and the particle size distributions in **(c)**.

ACPD
11, 16465–16497, 2011